


Critical Prandtl Number for Heat Transfer Enhancement in Rotating Convection

Mohammad Anas¹ and Pranav Joshi¹

Department of Mechanical Engineering, Indian Institute of Technology, Kanpur 208016, India

 (Received 18 July 2023; revised 25 November 2023; accepted 19 December 2023; published 16 January 2024)

Rotation, which stabilizes flow, can enhance the heat transfer in Rayleigh-Bénard convection (RBC) through Ekman pumping. In this Letter, we present the results of our direct numerical simulations of rotating RBC, providing a comprehensive analysis of this heat transfer enhancement relative to nonrotating RBC in the parameter space of Rayleigh number (Ra), Prandtl number (Pr), and Taylor number (Ta). We show that for a given Ra, there exists a critical Prandtl number (Pr_{cr}) below which no significant heat transfer enhancement occurs at any rotation rate, and an optimal Prandtl number (Pr_{opt}) at which maximum heat transfer enhancement occurs at an optimal rotation rate (Ta_{opt}). Notably, Pr_{cr} , Pr_{opt} , Ta_{opt} , and the maximum heat transfer enhancement all increase with increasing Ra. We also demonstrate a significant heat transfer enhancement up to $Ra = 2 \times 10^{10}$ and predict that the enhancement would become even more pronounced at higher Ra, provided Pr is also increased commensurately.

DOI: [10.1103/PhysRevLett.132.034001](https://doi.org/10.1103/PhysRevLett.132.034001)

Thermal convection under the influence of background rotation manifests in various geophysical and astrophysical flows, such as flows occurring within the Earth's atmosphere, oceans, and outer core [1–3], gaseous planets like Jupiter [4,5], and solar interiors [6]. Rotation, which introduces the Coriolis force into the system, significantly affects the characteristics of these flows, including heat and momentum transfer [7,8]. The canonical model to study the behavior of such systems is rotating Rayleigh-Bénard convection (RBC), in which fluid motion occurs between a hot plate (at the bottom) and a cold plate (at the top) as a consequence of the thermal buoyancy while the system rotates along an axis parallel to the gravity [7].

Rotating RBC is primarily governed by three dimensionless parameters: the Rayleigh number (Ra), which represents the strength of the buoyancy force over the dissipative forces, the Prandtl number (Pr), which represents the ratio of the momentum diffusivity to thermal diffusivity, and the Taylor number (Ta), which represents the strength of the Coriolis force relative to the viscous force. To characterize the relative strength of convection over rotation, convective Rossby number ($Ro = \sqrt{Ra/Ta Pr}$) is commonly used. When $Ro \gg 1$, the buoyancy force dominates over the Coriolis force, and the heat transfer characteristics of rotating RBC systems are similar to those of corresponding nonrotating RBC [9–11]. On the other hand, when $Ro \ll 1$, rotation becomes dominant and the heat transfer in rotating RBC, as compared to that of nonrotating case, is severely suppressed. Such rotating RBC system exhibits similarities to geostrophic flow, which is characterized by a force balance between pressure gradient and the Coriolis force [9,12,13].

Rotation, which suppresses the intensity of flow, enhances the heat transfer in RBC for a certain range of Ra, Pr,

and Ta [8,11,14–28]. This heat transfer enhancement in rotating RBC as compared to the nonrotating case is ascribed to Ekman pumping. Rotation generates columnar vortices aligned with the rotation axis in the flow, which in turn induce a secondary motion (parallel to the rotation) within the viscous boundary layer [29]. This secondary motion facilitates the transport of hot fluid (at the bottom plate) and cold fluid (at the top plate) from the thermal boundary layers, leading to this enhancement in the heat transfer [13,19,30].

Although prior studies have reported the effect of Ra, Pr, and Ta (or $1/Ro$) on the heat transfer enhancement in rotating RBC [17,19,20,22,31], a clear understanding of the possible enhancement as a function of these parameters has been missing. In this Letter, we provide a systematic comprehensive analysis of the heat transfer enhancement in rotating RBC in the Ra, Pr, Ta parameter space. We explore a very wide range of Prandtl numbers, including very high Pr (~ 1000) that have not been studied earlier for rotating convection, to uncover the existence of a “critical” Prandtl number, Pr_{cr} . We show that for each Ra (at least within the range of $Ra = 2 \times 10^4 - 2 \times 10^{10}$ explored in the present work), a significant heat transfer enhancement will occur only if the Prandtl number is greater than Pr_{cr} that increases with increasing Ra. For a given Ra, we also provide a precise definition of the optimal Prandtl number Pr_{opt} at which the maximum heat transfer enhancement occurs at an optimal rotation rate, Ta_{opt} , and show that Pr_{opt} and Ta_{opt} also increase with increasing Ra. Furthermore, we demonstrate a significant heat transfer enhancement up to $Ra = 2 \times 10^{10}$ and predict even higher enhancement at higher Ra.

For this study, we perform direct numerical simulations of rotating RBC for a wide range of parameters:

$Ra = g\beta\Delta H^3/(\nu\kappa) = 2 \times 10^4 - 2 \times 10^{10}$, $Pr = \nu/\kappa = 1-1000$, and $Ta = 4\Omega^2 H^4/\nu^2 = 0-2 \times 10^{12}$, and measure the heat transfer in terms of the Nusselt number $Nu = qH/(\lambda\Delta)$. Here, g is the acceleration due to gravity, β is the thermal expansion coefficient, Δ is the temperature difference between the hot and cold plates, H is the separation between the plates, ν is the kinematic viscosity, κ is the thermal diffusivity, Ω is the system's rotation rate, λ is the thermal conductivity of the fluid, and q is the heat flux from the hot to cold plates. We perform simulations in a horizontally periodic rectangular domain of size $L \times L \times H$ ($L \times L$ in the horizontal directions) employing isothermal and no-slip (and impenetrable) boundary conditions at the top (cold) and bottom (hot) plates. For the simulations of nonrotating RBC ($Ta = 0$) at moderate Ra , we use large aspect ratio ($\Gamma = L/H$) to avoid the effect of confinement on the Nusselt number [32]: $\Gamma = 8$ for $Ra = 2 \times 10^4 - 10^6$ and $\Gamma = 4$ for $Ra = 10^7 - 10^8$. Considering the high computational cost at large Γ for high Ra , we use $\Gamma = 1$ for $Ra = 5 \times 10^8 - 2.3 \times 10^9$ and $\Gamma = 0.5$ for $Ra = 10^{10}$. To obtain Nu at $Ra = 2 \times 10^{10}$ for nonrotating RBC, we fit the available Nu data in the range $Ra = 10^6 - 10^{10}$ to a power law and estimate the following values: $Nu \approx 0.114Ra^{0.304} \approx 154$ for $Pr = 20$, $Nu \approx 0.131Ra^{0.298} \approx 154$ for $Pr = 50$, and $Nu \approx 0.122Ra^{0.301} \approx 154$ for $Pr = 100$.

Since the horizontal length scale of the flow in rotating convection, ℓ , decreases with Ta , as $\ell \approx 0.9 Ta^{-1/6}H$ [33], we use relatively lower aspect ratios (half or one-fourth of those for the corresponding nonrotating RBC cases) for some simulations of rotating RBC. In all simulations of rotating RBC, we ensure that $\ell/L < 1/10$ (and also $\ell_c/L \lesssim 1/8$), which is sufficient to mitigate the effect of confinement on Nu [30,34]. Here, $\ell_c \approx 2.4 Ta^{-1/6}H$ is the horizontal length scale that develops at the onset of convection in rotating RBC for $Pr \gtrsim 0.68$ [7,13]. For more details about the simulations and the solver used in this study, please refer to the Supplemental Material [35].

In Fig. 1, we show the variation of the normalized Nusselt number Nu/Nu_0 (Nu_0 is the Nusselt number for the nonrotating case) with the Taylor number, Ta , and the inverse of the Rossby number, $1/Ro$, for $Pr = 1-1000$ at $Ra = [10^7, 10^8, 10^9, 10^{10}]$. We observe that when Pr is not too small, Nu/Nu_0 first increases and then decreases as the rotation rate is increased. For each Ra , the maximum enhancement in the heat transfer as compared to the nonrotating case occurs in a certain range of Pr and rotation rate. This maximum enhancement increases with increasing Ra and can reach up to approximately 25%, 40%, and 55% for $Ra = 10^7$, $Ra = 10^8$, and $Ra = 10^9$, respectively. Note that we observe more than 40% enhancement in heat transfer at $Ra = 10^{10}$, which will be discussed later in greater detail.

Interestingly, we observe that the Taylor number Ta serves as a better parameter than $1/Ro$ in representing the

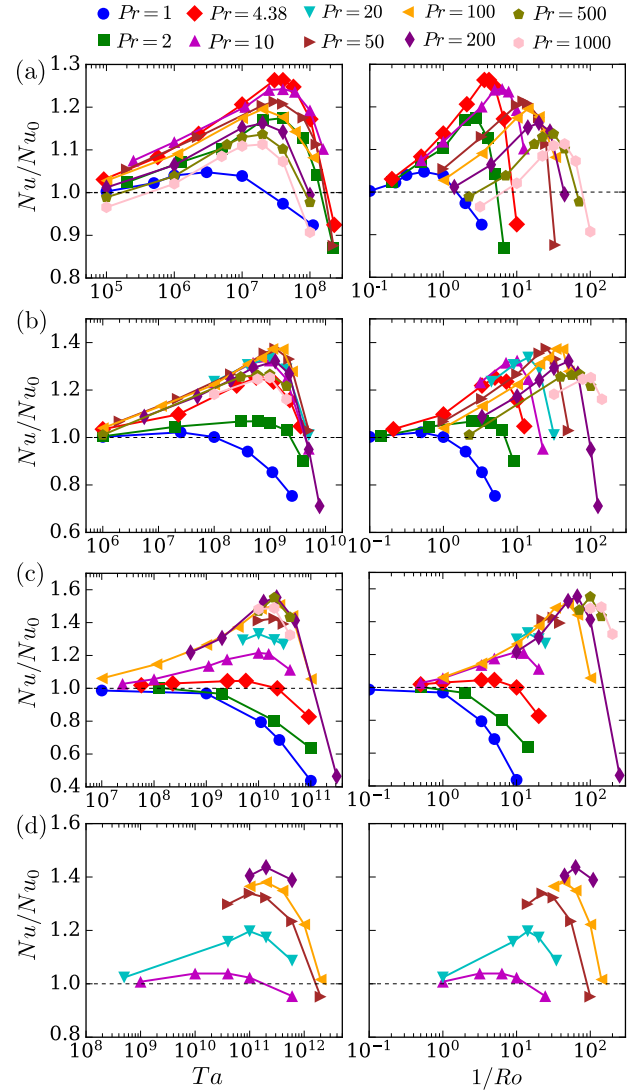


FIG. 1. Variation of the normalized Nusselt number Nu/Nu_0 with Taylor number Ta (left) and $1/Ro$ (right) for various Pr at (a) $Ra = 10^7$, (b) $Ra = 10^8$, (c) $Ra = 10^9$, and (d) $Ra = 10^{10}$. Solid lines are used to connect data points, aiding visual interpretation.

optimal rotation rate at which the maximum enhancement occurs (see Fig. 1). Unlike the optimal rotation rate represented in terms of the inverse of Rossby number, $(1/Ro_{opt})$, the optimal Taylor number, Ta_{opt} , is nearly independent of Pr when a significant enhancement is observed at a given Ra . Most earlier studies used $1/Ro_{opt}$ to represent the optimal rotation rate but found $1/Ro_{opt}$ to be strongly dependent on Pr [19,20,22]. Since the heat transfer enhancement due to rotation is largely controlled by the dynamics of the Ekman boundary layer [45], the thickness of which depends only on the Taylor number (which represents the ratio of Coriolis to viscous forces), Ta can be expected to represent better the heat transfer enhancement than $1/Ro$ (which represents the ratio of Coriolis to

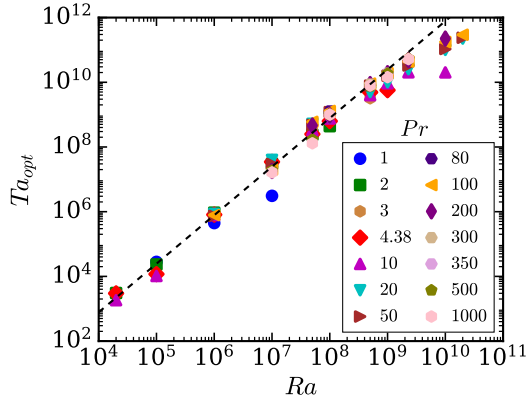


FIG. 2. Variation of the optimal Taylor number Ta_{opt} with Ra for various Pr . Dashed line represents $Ta_{opt} = 0.02 Ta_{cs}$, where $Ta_{cs} = (Ra/8.7)^{1.5}$.

buoyancy forces) at moderate and high rotation rates. This finding is also in line with the hypothesis of King *et al.* [9] that the boundary layer controls the rotation-dominated regime in rotating RBC, rather than the balance between the buoyancy and Coriolis forces. Nonetheless, the beginning of the rotation-affected regime, i.e., the rotation rate at which Nu/Nu_0 starts deviating from 1, is better represented by $1/Ro$ than by Ta , as seen from our results. Specifically, for $Ra = 10^7$ and 10^8 , the rotation-affected regime begins at $1/Ro \approx 0.2$, while for $Ra = 10^9$, it begins at $1/Ro \approx 0.4$. These values are consistent with the findings of Stevens *et al.* [11].

In Fig. 2, we show the variation of Ta_{opt} with Ra for various Prandtl numbers. As discussed earlier, we observe that at a given Ra , the optimal Taylor number does not vary significantly with Pr . Also, Ta_{opt} follows a power law close to $Ta_{opt} \propto Ra^{1.5}$ up to a certain Ra and this limiting Ra for the power law seems to increase with increasing Pr . Note that the Taylor number at which rotating RBC transitions from a convective state to a conductive state (Ta_{cs}) also follows the scaling $Ta_{cs} \propto Ra^{1.5}$ for $Pr \gtrsim 0.68$ and $Ta \gg 0$ [7,13]. Similar to Ta_{cs} , it is plausible that Ta_{opt} also signifies a regime transition in rotating RBC that occurs at $Ta_{opt} \sim 0.02 Ta_{cs}$ (see Fig. 2).

In Fig. 3, we show the variation of the normalized maximum Nusselt number, Nu_{max}/Nu_0 , with Pr for $Ra = 2 \times 10^4 - 2 \times 10^{10}$. At any given Ra and Pr , Nu_{max} , by definition, corresponds to the Nusselt number at the optimal Taylor number for that Ra and Pr . The maximum heat transfer enhancement represented by Nu_{max}/Nu_0 for each Ra increases with Pr up to a certain Pr and then decreases. Note that for each Ra there exists a Prandtl number (obtained by extrapolating the data for each Ra to $Nu_{max}/Nu_0 = 1$) below which there will be no (or marginal) heat transfer enhancement at any rotation rate. We call this Pr the critical Prandtl number Pr_{cr} . In rotating convection, columnar vortical structures are known to play

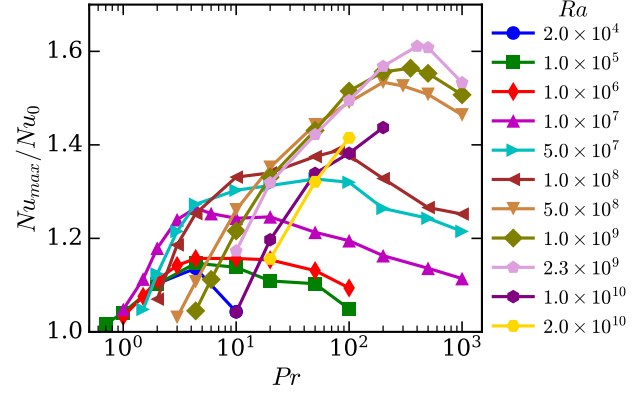


FIG. 3. Variation of the normalized maximum Nusselt number Nu_{max}/Nu_0 with Pr for various Ra .

an important role in the heat transfer by transporting the temperature anomaly from the hot (cold) wall to the cold (hot) wall [19,30]. However, for $Pr < Pr_{cr}$, it is likely that the lateral diffusion of the heat or temperature anomaly away from the vortex columns restricts their ability to transport heat between the top and bottom walls [22,31]: see the contours of the temperature field for $Pr = 1$ in Fig. 4, which shows the instantaneous flow structures for various Pr at $Ra = 10^8$ and $Ta \approx 10^9$. Note that for $Ra = 10^8$, $Pr_{cr} \approx 2$, $Pr_{opt} \sim 100$ (discussion on Pr_{opt} follows), and $Ta_{opt} \sim 10^9$. As Pr increases, this effect is expected to weaken [e.g., see the contours of the temperature field in Figs. 4(b) and 4(c)], and so the heat transfer enhancement increases. However, the heat transfer enhancement decreases again at very large Pr . At any Ra , we define the Prandtl number at which Nu_{max}/Nu_0 reaches its maximum as the optimal Prandtl number Pr_{opt} for that Ra . Some studies (e.g., Stevens *et al.* [22]), comparing the heat transfer at a constant Ro , have proposed that at large Pr , the Ekman boundary layer (δ_u) is significantly thicker than the thermal boundary layer (δ_θ); consequently, the columnar vortices do not reach the thermal boundary layer and the fluid entering them is not as hot (or as cold), leading to a decrease in the heat transfer enhancement at large Pr . However, we observe that the maximum enhancement (which occurs at Ta_{opt}) decreases at large Prandtl number even though $1.3 \lesssim \delta_u/\delta_\theta \lesssim 1.5$ for $Pr > Pr_{opt}$ (see Supplemental Material [35]).

Currently, we lack a concrete explanation for the existence of Pr_{opt} . However, to gain a preliminary understanding of the effect of Pr on Ekman pumping and, consequently, on the heat transfer enhancement, we present the contours of the vorticity component in the direction of rotation (z vorticity) along with the contours of the temperature fields in Fig. 4. Note that the normalized z vorticity, $\hat{\omega}_z = \sqrt{(Pr/Ra)}\omega_z$, serves as a proxy for the strength of Ekman pumping [29]. It is clear that similar to the heat transfer enhancement, the strength of Ekman pumping (represented by $\hat{\omega}_z$) reaches a maximum at $Pr \sim Pr_{opt}$. Importantly, rotation seems to change profoundly the effect

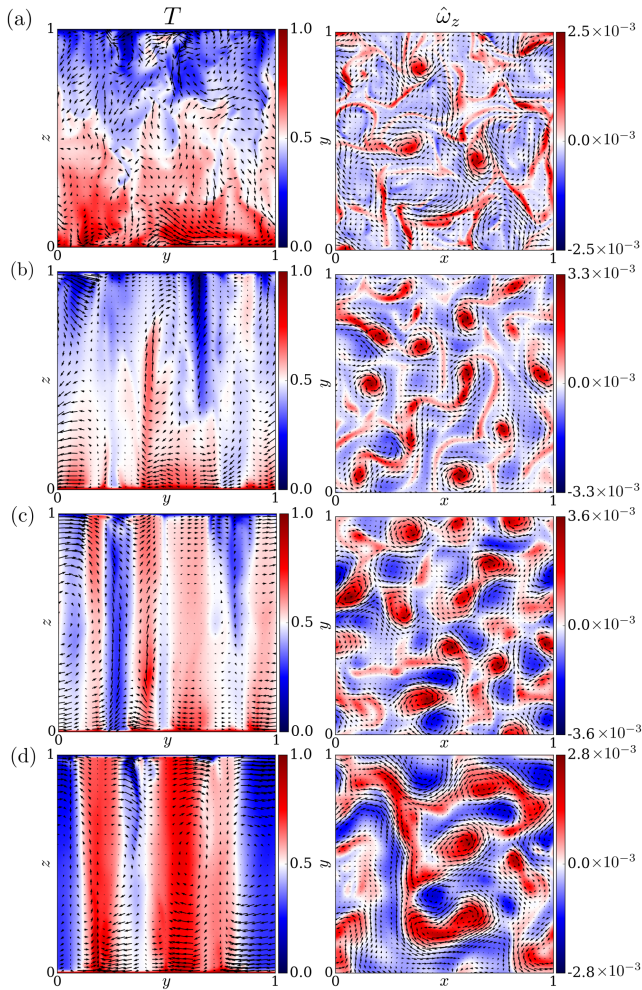


FIG. 4. Instantaneous contours of the normalized temperature field T in the yz plane at $x = L/2$ (left) and the normalized z -vorticity field, $\hat{\omega}_z = \sqrt{(\text{Pr}/\text{Ra})}\omega_z$, in the xy plane at $z \approx 1.2\delta_u$ (right) with superimposed velocity vectors for (a) $\text{Pr} = 1$, (b) $\text{Pr} = 4.38$, (c) $\text{Pr} = 100$, and (d) $\text{Pr} = 1000$ at $\text{Ra} = 10^8$ and $\text{Ta} \approx \text{Ta}_{\text{opt}}$. Note that the rotation axis is along z direction and for $\text{Ra} = 10^8$, $\text{Pr}_{\text{cr}} \approx 2$ and $\text{Pr}_{\text{opt}} \sim 100$.

of Pr on convection. At high Pr , a significant difference exists between the scales of the temperature and vorticity fields in nonrotating convection [46] (also see Fig. S5 in Supplemental Material [35]). However, as evident in Fig. 4(d) and Fig. S5 of [35], in rotating convection the temperature field maintains a high degree of coherence with z vorticity. Consequently, the lateral spatial scales of the temperature field exhibit a substantial increase as Pr increases beyond Pr_{opt} and are likely to be associated with a decrease in the heat transfer enhancement in comparison to nonrotating convection.

Now, we make an important observation. Our results show a significant heat transfer enhancement compared to nonrotating RBC at $\text{Ra} = 10^{10}$ ($\approx 43\%$ for $\text{Pr} = 200$) and $\text{Ra} = 2 \times 10^{10}$ ($\approx 41\%$ for $\text{Pr} = 100$), and the trends

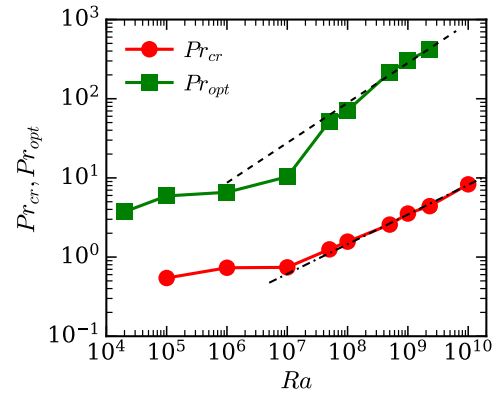


FIG. 5. Variation of the critical Prandtl number Pr_{cr} and the optimal Prandtl number Pr_{opt} with Ra . Dot-dashed and dashed lines represent power-law fits $\text{Pr}_{\text{cr}} \approx 1.46 \times 10^{-3} \text{Ra}^{0.375}$ in the range $\text{Ra} = 10^7 - 10^{10}$ and $\text{Pr}_{\text{opt}} \approx 8.18 \times 10^{-3} \text{Ra}^{0.504}$ in the range $\text{Ra} = 10^6 - 2.3 \times 10^9$, respectively.

(see Fig. 3) suggest an even more pronounced enhancement for higher Pr (up to the respective Pr_{opt}). Earlier, Weiss *et al.* [27] also reported the heat transfer enhancement at $\text{Ra} \sim 10^{10}$ for $\text{Pr} = 4.38 - 35.5$. However, the enhancement observed in their study, ($\approx 4\% - 17\%$), is significantly lower than that in the present study because of their lower Pr (closer to Pr_{cr}) and, in some cases, lower Ta ($< \text{Ta}_{\text{opt}}$). The present results predict that a significant heat transfer enhancement in rotating RBC is possible at high Ra , provided Pr is substantially higher (closer to Pr_{opt}) than Pr_{cr} . Since most earlier studies commonly employed air ($\text{Pr} \sim 1$) or water ($\text{Pr} \approx 4 - 7$) as the working fluid, for example, Niemela *et al.* [47] ($\text{Pr} = 0.7 - 5.9$), Stellmach *et al.* [45] ($\text{Pr} \approx 1 - 7$), Kunnen *et al.* [34] ($\text{Pr} = 1$), Ecke and Niemela [48] ($\text{Pr} = 0.7$), and Hartmann *et al.* [31] ($\text{Pr} = 4.38$ and 6.4), they failed to observe any (or significant) heat transfer enhancement at $\text{Ra} \gtrsim 10^{10}$, for which $\text{Pr}_{\text{cr}} \gtrsim 10$. Note that we also observe a significant heat transfer enhancement ($> 10\%$) at $\text{Ra} = 2 \times 10^4$ (using $\Gamma = 8$), in agreement with Rossby's experimental results [8] for $\Gamma \gtrsim 6$.

In Fig. 5, we show the variation of Pr_{cr} and Pr_{opt} with Ra . Interestingly, both Pr_{cr} and Pr_{opt} increase monotonically with Ra and approximately follow power laws: $\text{Pr}_{\text{cr}} \approx 1.46 \times 10^{-3} \text{Ra}^{0.375}$ and $\text{Pr}_{\text{opt}} \approx 8.18 \times 10^{-3} \text{Ra}^{0.504}$. Considering the high computational cost at large Pr and large Ra , we do not perform simulations at $\text{Pr} > 200$ and $\text{Pr} > 100$ to find Pr_{opt} for $\text{Ra} = 10^{10}$ and $\text{Ra} = 2 \times 10^{10}$, respectively, which are estimated to be $\text{Pr}_{\text{opt}} \sim 1000$ by the above power-law fit. As Rayleigh number increases, the turbulent diffusion of heat is also expected to become stronger. At low Pr , this higher turbulent diffusion will combine with the large molecular thermal diffusivity to further increase the lateral diffusion of heat in the bulk, and hence, will decrease the ability of the vortex columns to transport heat. Thus, a

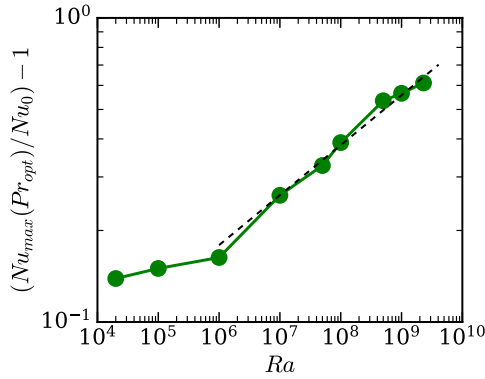


FIG. 6. Variation of $[\text{Nu}_{\max}(\text{Pr}_{\text{opt}})/\text{Nu}_0] - 1$ with Ra . Dashed line represents power-law fit $\text{Nu}_{\max}(\text{Pr}_{\text{opt}})/\text{Nu}_0 \approx 1 + 0.0185 Ra^{0.164}$ in the range $Ra = 10^6 - 2.3 \times 10^9$.

correspondingly larger Pr may be necessary to counter this effect of the enhanced turbulent thermal diffusivity to register any enhancement in the heat transfer, i.e., Pr_{cr} will increase with increasing Ra . On the other hand, as the buoyancy forcing increases with increasing Ra , the effects of large Pr will diminish and the heat transfer enhancement can be sustained until larger Prandtl numbers, i.e., Pr_{opt} also increases as Ra is increased.

In Fig. 6, we show the variation of $[\text{Nu}_{\max}(\text{Pr}_{\text{opt}})/\text{Nu}_0] - 1$ with Ra . Here, $\text{Nu}_{\max}(\text{Pr}_{\text{opt}})$ is Nu_{\max} at $\text{Pr} = \text{Pr}_{\text{opt}}$. Similar to Pr_{cr} and Pr_{opt} , $[\text{Nu}_{\max}(\text{Pr}_{\text{opt}})/\text{Nu}_0] - 1$ also increases with increasing Ra , and the trend can be fitted by a power law $\text{Nu}_{\max}(\text{Pr}_{\text{opt}})/\text{Nu}_0 \approx 1 + 0.0185 Ra^{0.164}$ in the range $Ra = 10^6 - 2.3 \times 10^9$. This relationship predicts that the maximum heat transfer enhancement increases with increasing Ra , provided the Prandtl number is also increased commensurately to the respective Pr_{opt} . In particular, the present results predict $\text{Nu}_{\max}/\text{Nu}_0 \approx 1.8$ (i.e., a maximum heat transfer enhancement of 80%) for $Ra = 10^{10}$ at $\text{Pr}_{\text{opt}} \approx 900$, and even higher maximum enhancement at $Ra > 10^{10}$ at higher Pr . As discussed earlier, Pr_{opt} increases with Ra , i.e., the increase in the heat transfer enhancement with increasing Pr can be sustained up to a larger Pr at higher Ra . Thus, the maximum enhancement can also be expected to increase with Ra .

Note that, due to the effect of finite aspect ratio on Nu in nonrotating simulations (mainly for $Ra \geq 5 \times 10^8$ in this work) [32], and owing to possible errors associated with the interpolation and extrapolation, there may be some uncertainty in the present values of Pr_{cr} , Pr_{opt} , and the maximum enhancement. However, this effect is expected to not alter any of the major findings of this study.

In conclusion, this work provides a clear picture of the heat transfer enhancement due to Ekman pumping in rotating Rayleigh-Bénard convection (RBC) as a function of Ra , Pr , and Ta . At a given Ra , we demonstrate the existence of a critical Prandtl number below which no

significant heat transfer enhancement can occur and an optimal Prandtl number at which the maximum enhancement is obtained. Both critical and optimal Prandtl numbers increase with increasing Ra . Importantly, our results show that the maximum enhancement also increases with Ra , provided Pr is increased commensurately. At present, we do not know up to what Ra these trends will persist. Simulations and experiments at significantly higher Ra and Pr than currently feasible may be required to answer this question.

Note that, similar to rotation, lateral confinement and a vertical magnetic field also stabilize flow and can also enhance the heat transfer in RBC [28,32,49,50]. Perhaps a systematic study of the effects of lateral confinement and a vertical magnetic field on the heat transfer in RBC will also reveal the existence of critical and optimal Prandtl numbers for these problems. In closing, we want to emphasize that by systematically exploring the heat transfer over a wide range of parameters, we believe that our study establishes a benchmark for testing and developing new models for rotating RBC.

For all the simulations related to this work, we gratefully acknowledge the support and the resources provided by Param Sanganak under the National Supercomputing Mission, Government of India at the Indian Institute of Technology, Kanpur. Access to the computational facility was partially supported by the Department of Science and Technology, Government of India, under Projects No. CRG/2022/008483 and No. DST/PHY/2020455. We also thank Professor M. K. Verma for inspiring us to utilize GPUs for scientific computing, and also for providing resources for the testing of the solver and for running some simulations. M. A. thanks Roshan Samuel for his valuable assistance in the development of the solver, as well as Soumyadeep Chatterjee, Shadab Alam, and Manthan Verma for their useful discussions on the solver and this work.

-
- [1] A. E. Gill, *Atmosphere–Ocean Dynamics* (Academic Press, New York, 1982).
 - [2] G. A. Glatzmaier and P. H. Roberts, *Nature (London)* **377**, 203 (1995).
 - [3] J. Marshall and F. Schott, *Rev. Geophys.* **37**, 1 (1999).
 - [4] A. P. Ingersoll, *Science* **248**, 308 (1990).
 - [5] M. Heimpel, J. Aurnou, and Wicht, *Nature (London)* **438**, 193 (2005).
 - [6] E. A. Spiegel, *Annu. Rev. Astron. Astrophys.* **9**, 323 (1971).
 - [7] S. Chandrasekhar, *Hydrodynamic and Hydromagnetic Stability* (Oxford University Press, Oxford, 1961).
 - [8] H. T. Rossby, *J. Fluid Mech.* **36**, 309 (1969).
 - [9] E. M. King, S. Stellmach, J. Noir, U. Hansen, and J. M. Aurnou, *Nature (London)* **457**, 301 (2008).
 - [10] E. M. King, S. Stellmach, and J. M. Aurnou, *J. Fluid Mech.* **691**, 568 (2012).

- [11] R. J. A. M. Stevens, J.-Q. Zhong, H. J. H. Clercx, G. Ahlers, and D. Lohse, *Phys. Rev. Lett.* **103**, 024503 (2009).
- [12] R. P. J. Kunnen, *J. Turbul.* **22**, 267 (2021).
- [13] R. E. Ecke and O. Shishkina, *Annu. Rev. Fluid Mech.* **55**, 603 (2023).
- [14] F. Zhong, R. E. Ecke, and V. Steinberg, *J. Fluid Mech.* **249**, 135 (1993).
- [15] Y. Liu and R. E. Ecke, *Phys. Rev. Lett.* **79**, 2257 (1997).
- [16] R. P. J. Kunnen, H. J. H. Clercx, and B. J. Geurts, *Phys. Rev. E* **74**, 056306 (2006).
- [17] R. J. Stevens, H. J. Clercx, and D. Lohse, *Eur. J. Mech. B* **40**, 41 (2013).
- [18] P. Wei, S. Weiss, and G. Ahlers, *Phys. Rev. Lett.* **114**, 114506 (2015).
- [19] J.-Q. Zhong, R. J. A. M. Stevens, H. J. H. Clercx, R. Verzicco, D. Lohse, and G. Ahlers, *Phys. Rev. Lett.* **102**, 044502 (2009).
- [20] Y. Yang, R. Verzicco, D. Lohse, and R. J. A. M. Stevens, *Phys. Rev. Fluids* **5**, 053501 (2020).
- [21] P. Vorobieff and R. E. Ecke, *J. Fluid Mech.* **458**, 191 (2002).
- [22] R. J. A. M. Stevens, H. J. H. Clercx, and D. Lohse, *New J. Phys.* **12**, 075005 (2010).
- [23] R. J. A. M. Stevens, H. J. H. Clercx, and D. Lohse, *Phys. Fluids* **22**, 085103 (2010).
- [24] R. J. A. M. Stevens, J. Overkamp, D. Lohse, and H. J. H. Clercx, *Phys. Rev. E* **84**, 056313 (2011).
- [25] P. Joshi, H. Rajaei, R. P. J. Kunnen, and H. J. H. Clercx, *J. Fluid Mech.* **830**, R3 (2017).
- [26] S. Weiss, R. J. A. M. Stevens, J.-Q. Zhong, H. J. H. Clercx, D. Lohse, and G. Ahlers, *Phys. Rev. Lett.* **105**, 224501 (2010).
- [27] S. Weiss, P. Wei, and G. Ahlers, *Phys. Rev. E* **93**, 043102 (2016).
- [28] K. L. Chong, Y. Yang, S.-D. Huang, J.-Q. Zhong, R. J. A. M. Stevens, R. Verzicco, D. Lohse, and K.-Q. Xia, *Phys. Rev. Lett.* **119**, 064501 (2017).
- [29] P. A. Davidson, *Turbulence in Rotating, Stratified and Electrically Conducting Fluids* (Cambridge University Press, Cambridge, England, 2013).
- [30] K. Julien, S. Legg, J. McWilliams, and J. Werne, *J. Fluid Mech.* **322**, 243 (1996).
- [31] R. Hartmann, G. S. Yerragolam, R. Verzicco, D. Lohse, and R. J. A. M. Stevens, *Phys. Rev. Fluids* **8**, 083501 (2023).
- [32] S.-D. Huang, M. Kaczorowski, R. Ni, and K.-Q. Xia, *Phys. Rev. Lett.* **111**, 104501 (2013).
- [33] E. M. King, S. Stellmach, and B. Buffett, *J. Fluid Mech.* **717**, 449 (2013).
- [34] R. P. J. Kunnen, R. Ostilla-Mónico, E. P. van der Poel, R. Verzicco, and D. Lohse, *J. Fluid Mech.* **799**, 413 (2016).
- [35] See Supplemental Material at <http://link.aps.org/supplemental/10.1103/PhysRevLett.132.034001> for the discussion related to the simulations and the solver, which includes Refs. [36–44].
- [36] P. G. Drazin and W. H. Reid, *Hydrodynamic Stability* (Cambridge University Press, Cambridge, England, 2004).
- [37] L. Cheng and S. Armfield, *Int. J. Numer. Methods Fluids* **21**, 15 (1995).
- [38] E. P. van der Poel, R. Ostilla-Mónico, J. Donners, and R. Verzicco, *Comput. Fluids* **116**, 10 (2015).
- [39] R. Samuel, S. Bhattacharya, A. Asad, S. Chatterjee, M. K. Verma, R. Samtaney, and S. F. Anwer, *J. Open Source Software* **6**, 2095 (2021).
- [40] P. R. Spalart, R. D. Moser, and M. M. Rogers, *J. Comput. Phys.* **96**, 297 (1991).
- [41] V. Eswaran and S. Pope, *Comput. Fluids* **16**, 257 (1988).
- [42] G. L. Kooij, M. A. Botchev, E. M. Frederix, B. J. Geurts, S. Horn, D. Lohse, E. P. van der Poel, O. Shishkina, R. J. Stevens, and R. Verzicco, *Comput. Fluids* **166**, 1 (2018).
- [43] G. Grötzbach, *J. Comput. Phys.* **49**, 241 (1983).
- [44] O. Shishkina, R. J. A. M. Stevens, S. Grossmann, and D. Lohse, *New J. Phys.* **12**, 075022 (2010).
- [45] S. Stellmach, M. Lischper, K. Julien, G. Vasil, J. S. Cheng, A. Ribeiro, E. M. King, and J. M. Aumou, *Phys. Rev. Lett.* **113**, 254501 (2014).
- [46] G. Silano, K. R. Sreenivasan, and R. Verzicco, *J. Fluid Mech.* **662**, 409 (2010).
- [47] J. J. Niemela, S. Babuin, and K. R. Sreenivasan, *J. Fluid Mech.* **649**, 509 (2010).
- [48] R. E. Ecke and J. J. Niemela, *Phys. Rev. Lett.* **113**, 114301 (2014).
- [49] K. L. Chong, S.-D. Huang, M. Kaczorowski, and K.-Q. Xia, *Phys. Rev. Lett.* **115**, 264503 (2015).
- [50] Z. L. Lim, K. L. Chong, G.-Y. Ding, and K.-Q. Xia, *J. Fluid Mech.* **870**, 519 (2019).